Report 2 on the PARIS Calorimeter Simulations

IPN Lyon, 69622 Villeurbanne, France
August 2007

Abstract

This work is a direct continuation of the study reported in [1]. Presently, we propose completing [1] by focusing on spatial energy deposit patterns, energy sharing between shells, etc.

1. Hit pattern

The distribution of the identification number of the shell which is fired *first* for a given incident γ-ray is displayed in Fig.1 for a two shell configuration with an inner LaBr3 shell between 10cm and 15cm and an outer CsI layer between 30cm and 45cm. The inner and outer shell are, respectively, numbered 1 and 2. For those events which deposit at least 95% of the incident energy in the detector ensemble (left panel of Fig.1), it is observed that up to 10MeV the number of events which first interaction point is located in the inner shell decreases. However, above E_{inc}=10MeV, most of the events deposit again energy along their *first* passage through the inner shell. This is most probably a consequence of (1) the dominance of pair creation as compared to Compton scattering above about 10MeV in LaBr3 and (2) the increasing pair creation cross section with increasing E_{inc} (cf. Appendix of [1]). Note that a first interaction point in the outer shell does not mean that the incident photon deposits only energy in the outer shell: energy can be lost in the inner shell at later stage by retro-diffused secondary particles. The robustness of the above conclusion depending on the characteristic of the event in terms of absorption is studied in the right panel of Fig.1: the hit pattern as function of energy remains similar whatever the percentage of energy deposited in the detector is. Some more curves are displayed for E_{inc}=10MeV in Fig.2 i.e. around the 'transition' regime for the transparency of the inner shell.

The influence of the thickness of the inner layer on the hit pattern is studied in figures 3 and 4. For a very thick (e.g. 10cm) inner LaBr3 layer, the inner shell is not transparent at all for most events whatever the energy. Yet, the number of events firing this shell along their first passage presents a minimum around E_{inc}=10MeV in accordance with above. At intermediate thickness (e.g. 5cm) and as mentioned previously, the inner shell becomes more transparent in the Compton scattering regime when E_{inc} increases, before becoming again quite absorbent when the cross section for the dominant pair creation is largest at highest energy. For small thickness (e.g. 3cm) the transparency of the inner shell for Compton scattering events occurs at lower E_{inc} as expected from the corresponding photon mean free path values (cf. Appendix of [1]). The increase of the interaction probability in the inner shell does persist in the pair creation regime when the energy increases, although first energy deposit mainly occurs in the outer shell. Only, at the highest energy (e.g. 40MeV) does the first interaction again mostly take place in the inner shell. This is related to the thickness of the inner shell that is

comparable to the mean free path of the photon in the material at such high energy. The 'degree' of transparency of the inner shell thus depends on its thickness.

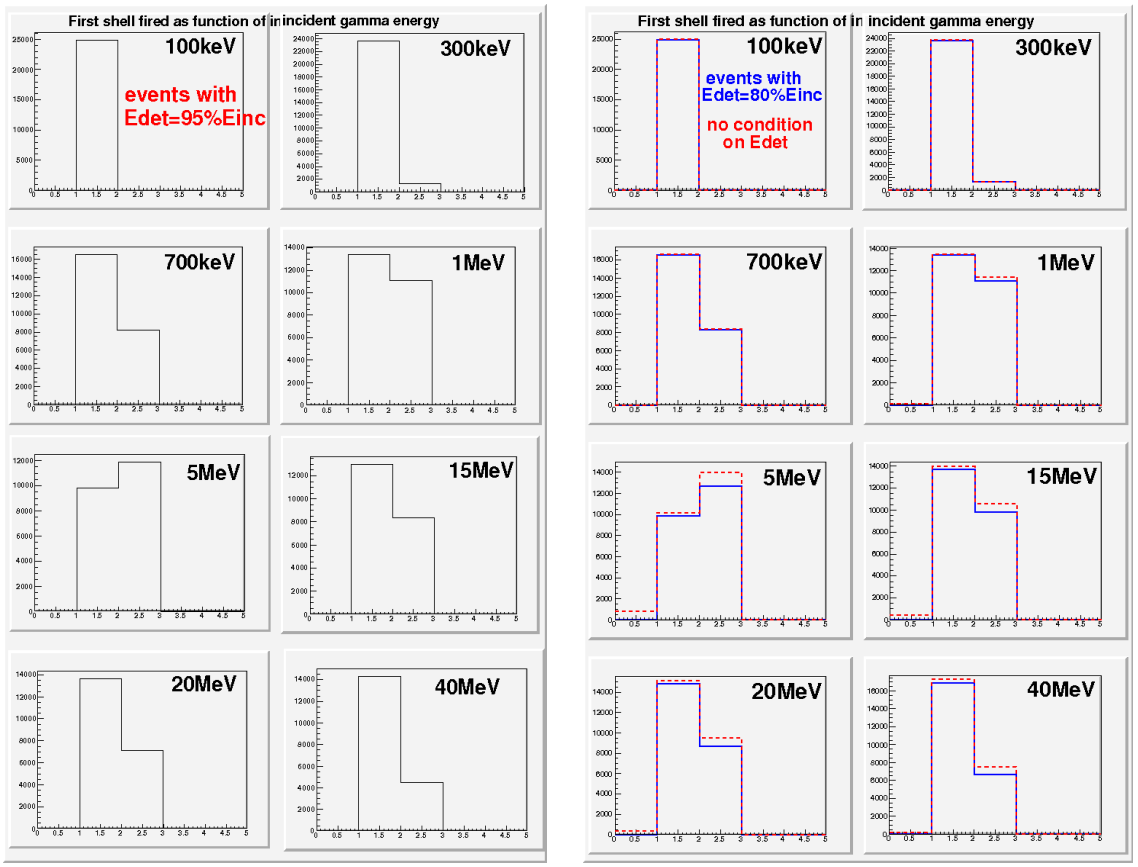

Fig. 1: Left panel: Distribution of the identification number of the shell which is fired first by a given incident photon with energies as indicated. Only those events depositing more than 95% of E_{inc} are included. The geometry corresponds to two-shell geometry with an inner LaBr3 layer with R_{in}=10cm and R_{out}=15cm followed by an outer CsI layer with R_{in}=30cm and R_{out}=45cm. Right panel: Similar to the left panel for events depositing more than 80% of E_{inc} and without condition on the energy deposit. For each energy, 25000 incident photons are simulated.

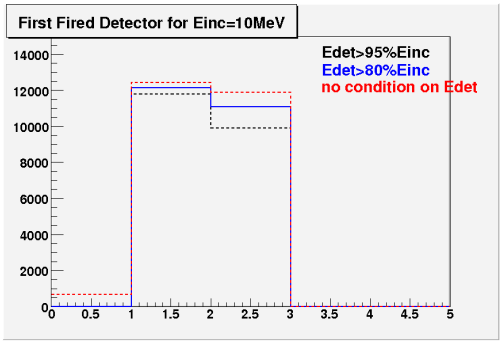

Fig. 2: Meaning of the curves similar to Fig.1for E_{inc}=10MeV.

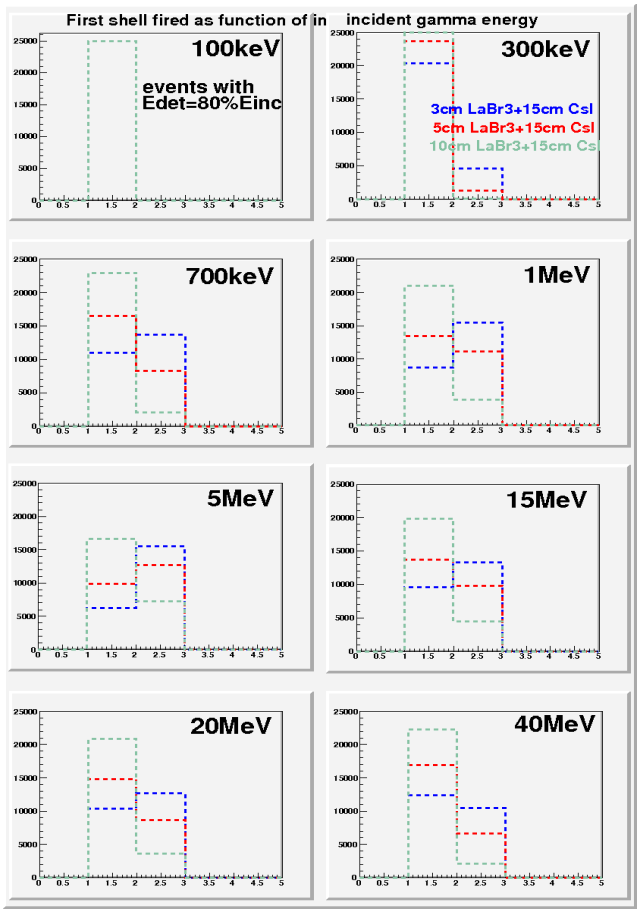

Fig. 3: Left panel: Distribution of the number of the shell which is fired first by a given incident photon with energies as indicated. Only those events depositing more than 80% of E_{inc} are included. Various configurations are considered for the thickness of the inner shell.

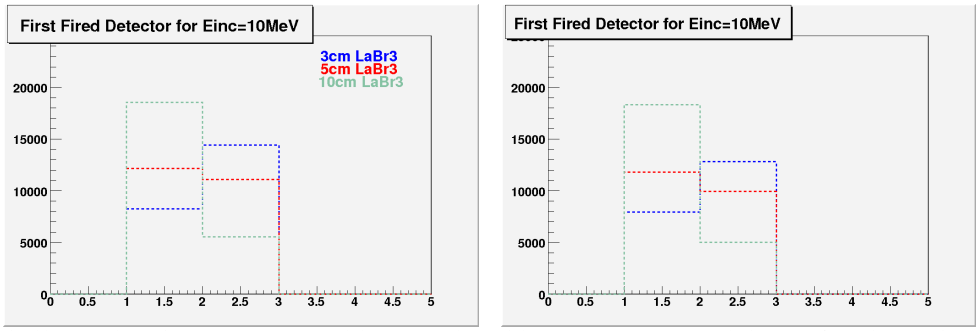

Fig. 4: Similar to Fig.3 for E_{inc}=10MeV with events depositing more than 80% (left) or 95% (right) of E_{inc}.

2. Energy partition

Aside from the location of the first and secondary interaction points generated by an incident photon, the amount of energy deposited at each step is as important. In addition to the preliminary investigations of [1], in the following the energy partition pattern in the inner and

outer shell is studied in close connection with the above hit pattern. This will be of help for determining the suited reconstruction algorithm.
The correlation between the energy deposited in the inner and the outer shell is displayed in Fig.5-8 and studied as function of the hit pattern of the event: Events which first interaction occurs either in the inner or in the outer shell are shown separately in the middle and right columns, respectively. Fig.5-8 differ in terms of absorption characteristics and thickness of the inner shell. The major part of the energy deposit is seen to occur in the shell which is fired first whatever the incident energy is. This observation holds independent on the thickness of the inner shell and whatever the final amount of energy absorbed is. A more detailed survey is given in Fig.9-10 by projecting some of the previous spectra on the *x*- and *y*- axis.

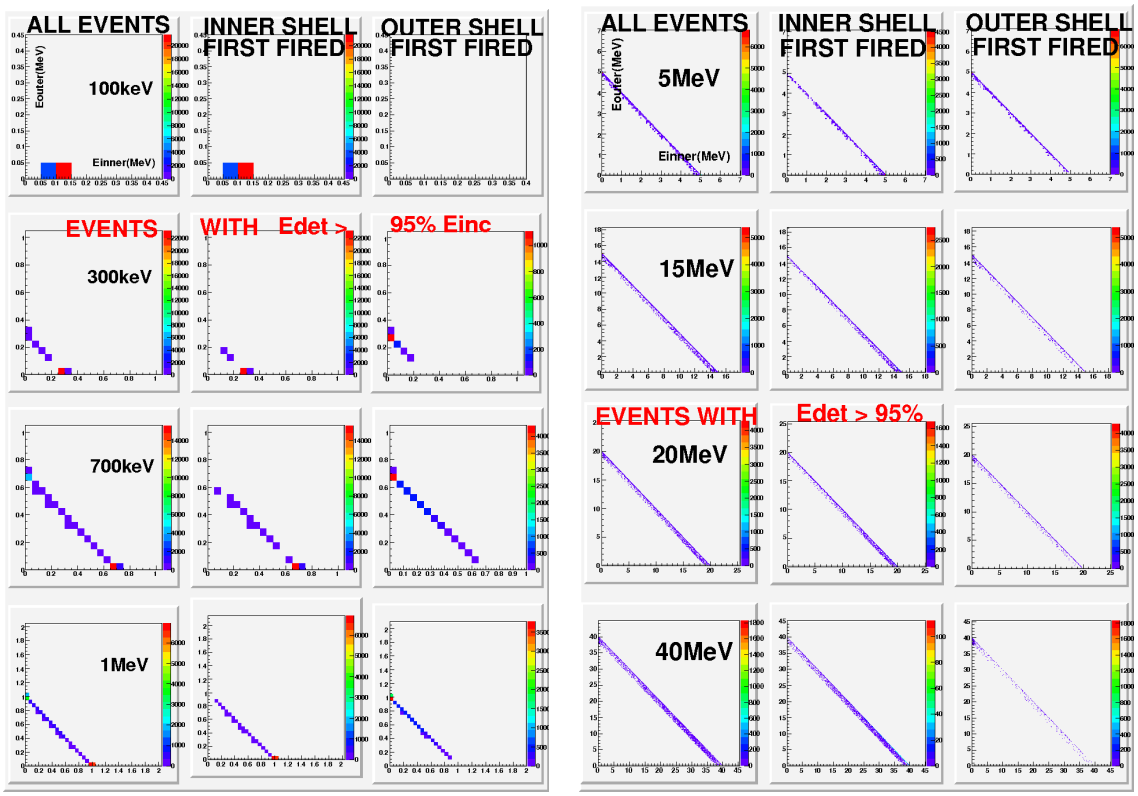

Fig. 5: Correlation between the energy deposit E_{inner} in the inner shell and the deposit E_{outer} in the outer shell for those events losing more than 95% of E_{inc} in the ensemble. Various incident photon energies are considered as indicated. A two-shell geometry with an inner LaBr3 layer with R_{in}=10cm and R_{out}=15cm followed by an outer CsI layer with R_{in}=30cm and R_{out}=45cm is considered. While the first column includes all events, the middle and right-most ones refer to events interacting first in the inner and outer shell, respectively. Note the linear z-scale.

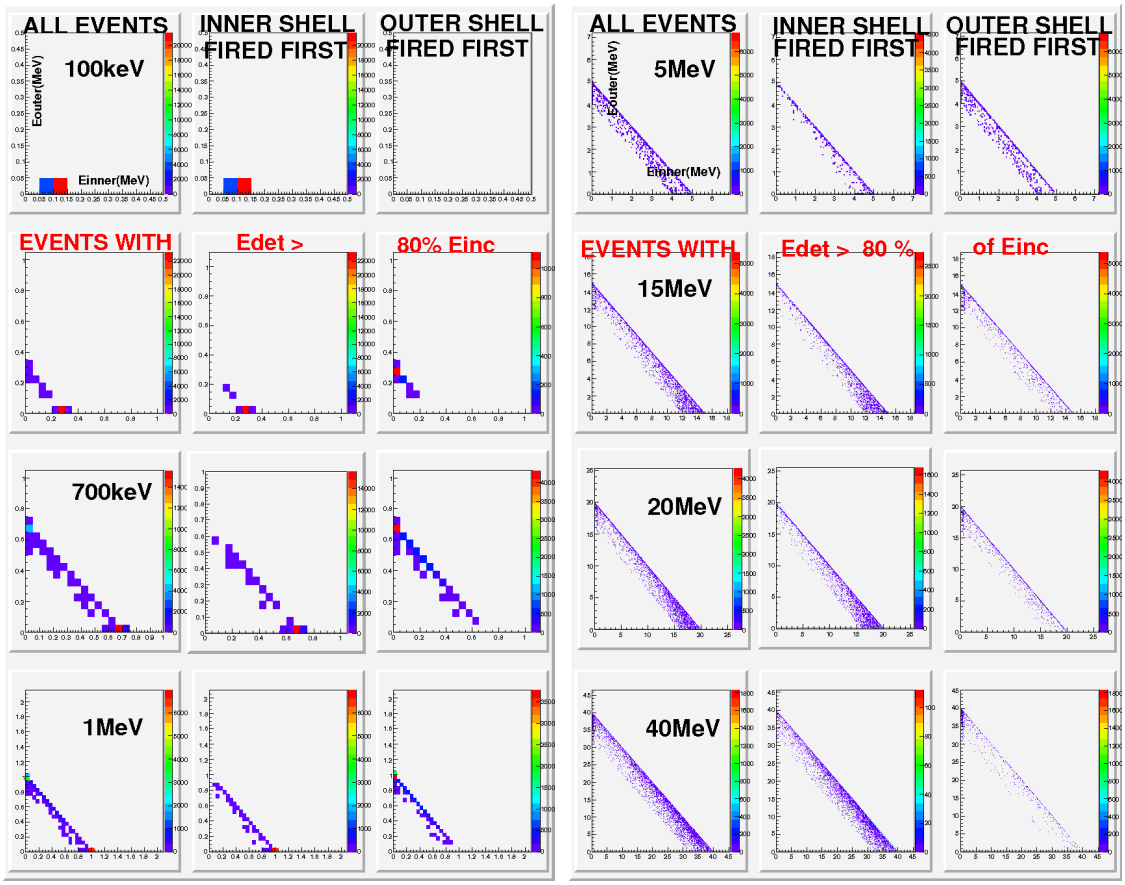

Fig. 6: Similar to Fig.5 for those events depositing more than 80% of E_{inc} in the detector ensemble.

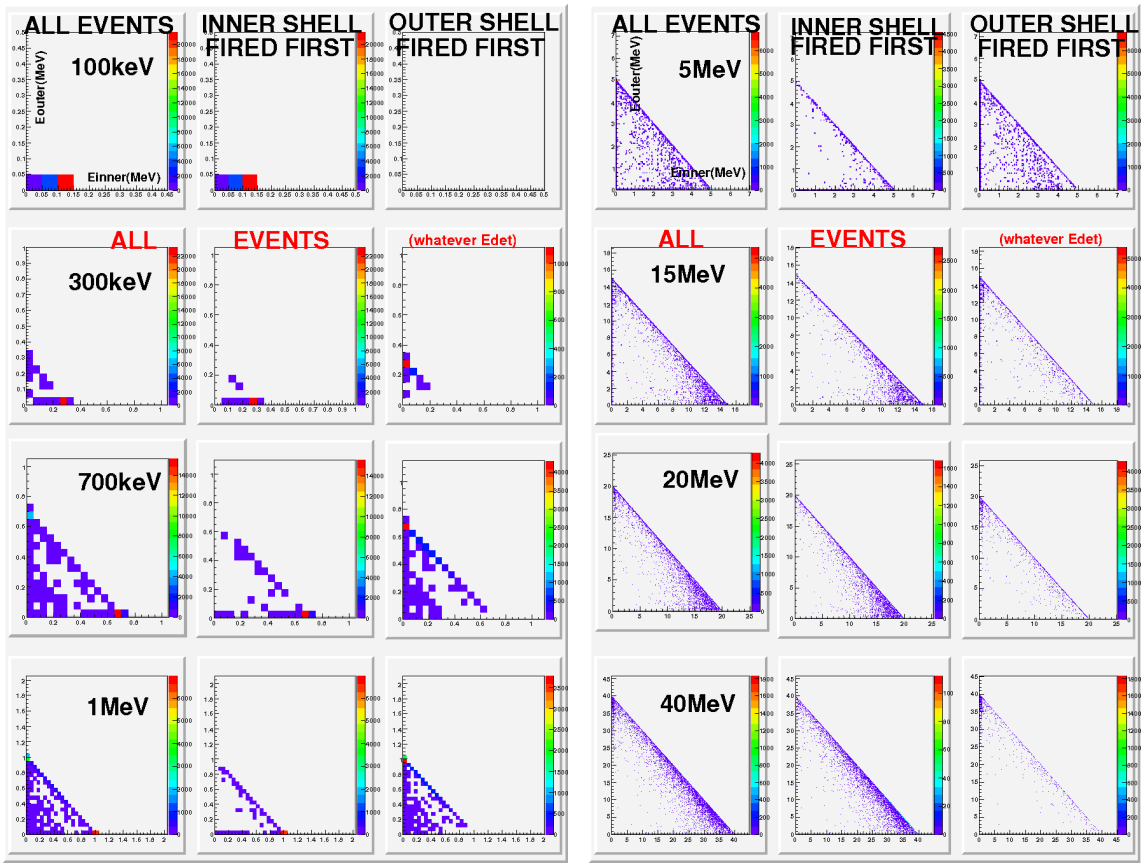

Fig. 7: Similar to Fig.5 without any condition on the percentage of energy deposit in the detector.

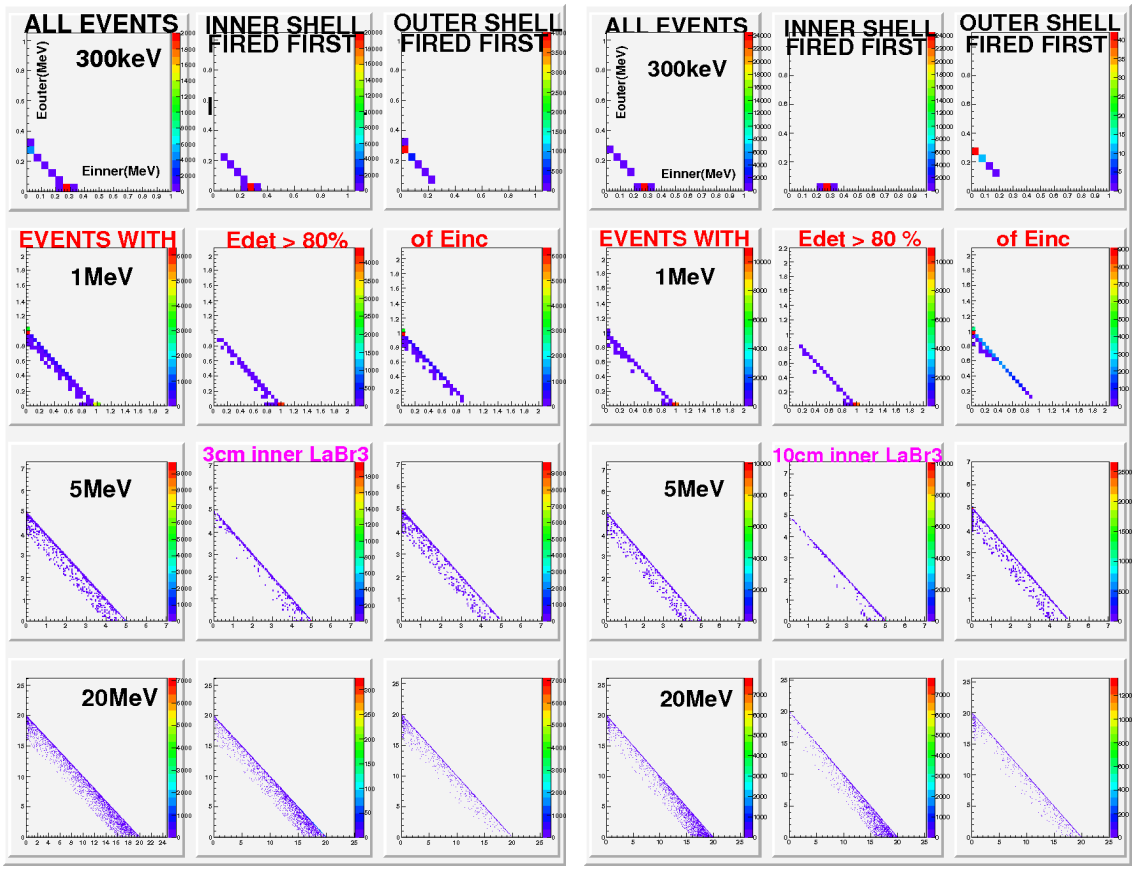

Fig. 8: Calculations scheme similar to Fig.6 for a few less E_{inc} and replacing the 5cm thick inner LaBr3 shell with a 3cm (left) and 10cm (right) thick layer.

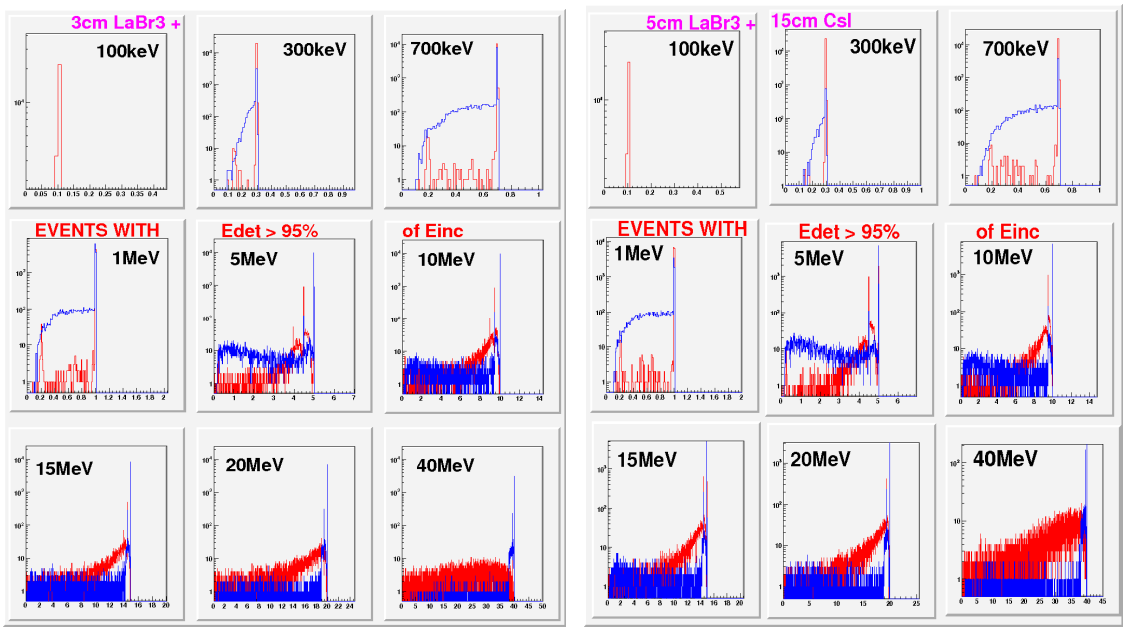

Fig. 9: Energy deposit in the inner shell for events where the inner shell is fired first (red histograms) and energy deposit in the outer shell for events where the outer shell is fired first (blue histogram). Various incident energies are considered as indicated. Only those events losing more than 95% of E_{inc} in the ensemble are taken into account. The geometry corresponds to a two-shell geometry with an inner LaBr3 layer followed by an outer CsI

layer with R_{in}=30cm and R_{out}=45cm. The left panel assumes an inner layer with R_{in}=10cm and R_{out}=13cm while the right panel refers to R_{in}=10cm and R_{out}=15cm.

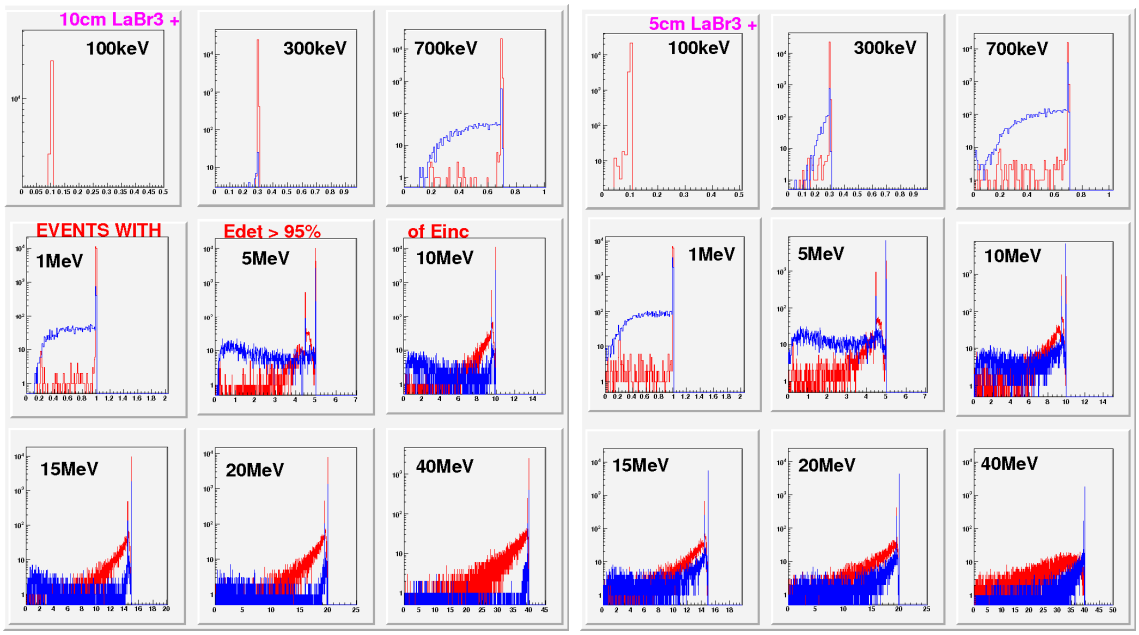

Fig. 10: Left panel: Identical to Fig.9 with R_{in}=10cm and R_{out}=20cm. Right panel: Identical to the right panel of Fig. 9 but without any condition on the amount of energy absorbed in the bulk of the detector.

The general trend in Fig.9 and 10 is independent on the thickness of the inner shell and the absorption criterion. Yet, in the range $E_{inc} \in$ [5-10]MeV, note the great number of events with escape from the inner shell of the two annihilation photons when the inner layer is particularly thin. In the Compton scattering domain up to a couple of MeV, when interacting first in the inner shell, the probability of depositing the whole amount of E_{inc} in the inner shell largely dominates. Conversely, when interacting first in the outer shell, the interaction might take place rather near to the inner surface of the outer layer. Thus, the probability for secondary particles for being scattered towards the inner shell is not negligible and some energy is deposited in the inner shell as well. With increasing incident energy, this trend changes. In the pair creation domain, the shower generated by the incident particle is more forward focused what decreases the probability of retro-diffusion from the outer to the inner shell [1] and energy partition between the two shells becomes negligible. Yet, diffusion from the inner to the outer shell remains valid, namely due to the escape of annihilation photon(s). These observations are corroborated by the relative intensity of the peaks at E_{inc} and (E_{inc}-511keV) in the inner as compared to the outer shell.

The fact that, even for the highest energy and the thinnest inner shell, in case the inner shell is fired first, the greatest part of the initial energy is still deposited in this layer is connected to the limited extent of the shower once weighted by the energy deposit [1]. This point might give some hope that most of the incident energy is deposited rather close to the first interaction point. Yet, the above figures do not contain any information on the proximity in space of the interaction points along the sequence of energy deposits. That will be further studied in forthcoming reports together with investigations on the segmentation.

3. Spatial extension of the shower

In order to determine the suited geometry and segmentation for each shell, the spatial (radial and longitudinal) extension of the shower generated by an incident photon with a given energy is crucial. Several quantities allowing to investigate the spatial shape of the shower have been introduced in [1]. In the following, some of them are used for studying how the shower depends on the distance *d* separating the two shells. In praxis, space has to be left there for the electronics (e.g. PMT's) of the inner shell. Below, we will more particularly focus on the extension of the shower in the outer shell depending on its shape in the inner shell and on the distance *d*. Figures 11-16 present the correlation between the radial ($\vec{r}\sin\ \vartheta$) and longitudinal ($\vec{r}\cos\ \vartheta$) dispersion including *all* interaction points generated by the incident photon. Each interaction point is weighted by the percentage of energy deposited at this point with respect to the incident energy. No condition on the amount of energy deposited in the detector bulk is applied. Several values are considered for *d* and the thickness of the inner shell. Fig. 11 includes all events while Fig. 12 is restricted to those events which first interaction occurs in the inner layer. In figures 13 and 14 the thickness of the inner shell is varied, and different values for *d* are considered in figures 15 and 16. In Fig.13-16 only those events which first interaction takes place in the inner shell are taken into account. This set of simulations is dedicated to study whether it is either the distance *d* or the shape of the shower at the outer/exit frontier of the inner shell (i.e. basically connected to the thickness of the inner shell) that determines primarily the extension of the shower in the outer shell. Aside from giving insight into the effect of *d*, such results are also of interest help for determining the segmentation of the inner vs. outer shell.

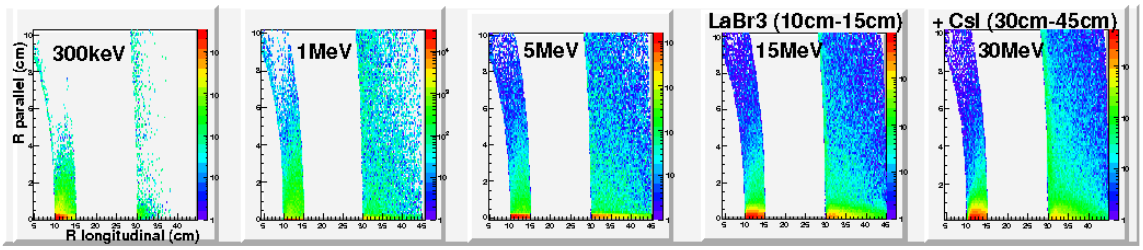

Fig. 11: Correlation between the longitudinal $R_{\perp}$ and parallel $R_{//}$ radius (in cm) of all interaction points generated by an incident photon with a given energy. Each point is weighted by the percentage of energy deposit with respect to the incident energy. No condition is required for the amount E_{det} of energy deposited in the detector. The geometry corresponds to a two-shell geometry with an inner LaBr3 layer with R_{in}=10cm and R_{out}=15cm followed by an outer CsI layer with R_{in}=30cm and R_{out}=45cm.

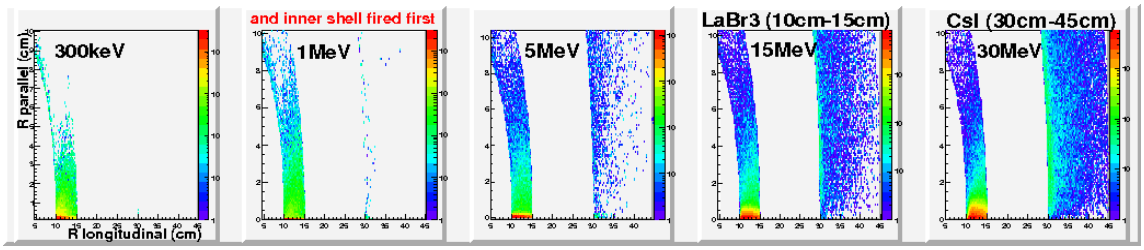

Fig. 12: Identical to Fig.11 for those events which first interaction point is located in the inner shell.

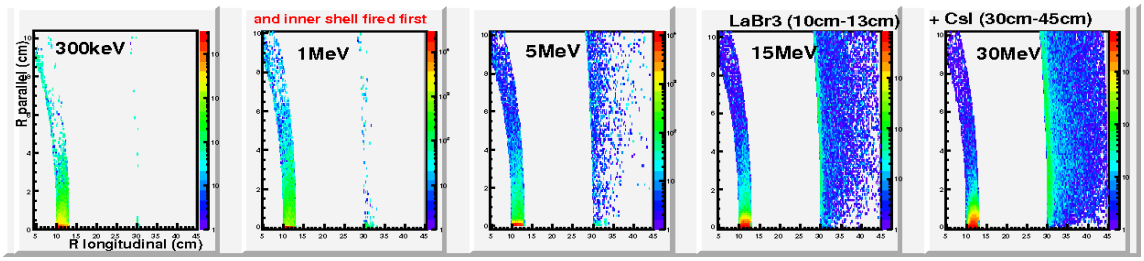

Fig. 13: Identical to Fig.12 for a two-shell geometry with an inner LaBr3 layer with R_{in}=10cm and R_{out}=13cm followed by an outer CsI layer with R_{in}=30cm and R_{out}=45cm.

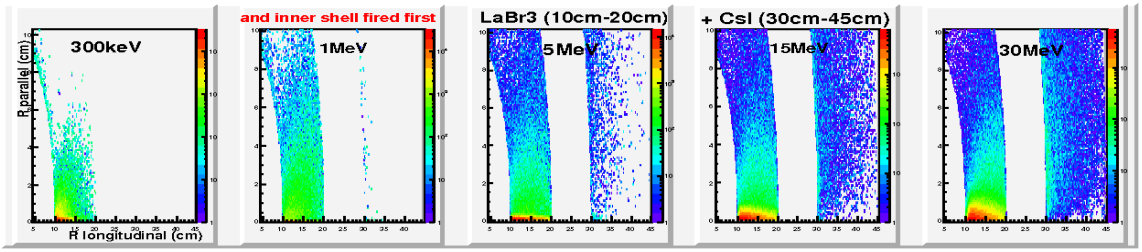

Fig. 14: Identical to Fig.12 for a two-shell geometry with an inner LaBr3 layer with R_{in}=10cm and R_{out}=20cm followed by an outer CsI layer with R_{in}=30cm and R_{out}=45cm.

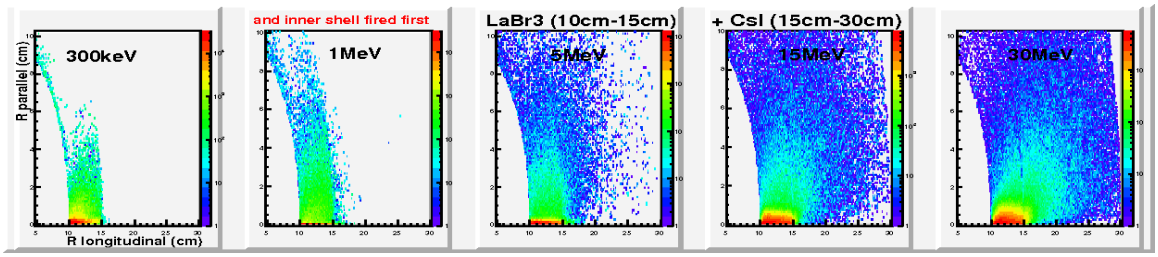

Fig. 15: Identical to Fig.12 for a two-shell geometry with an inner LaBr3 layer with R_{in}=10cm and R_{out}=15cm followed by an outer CsI layer with R_{in}=15cm and R_{out}=30cm.

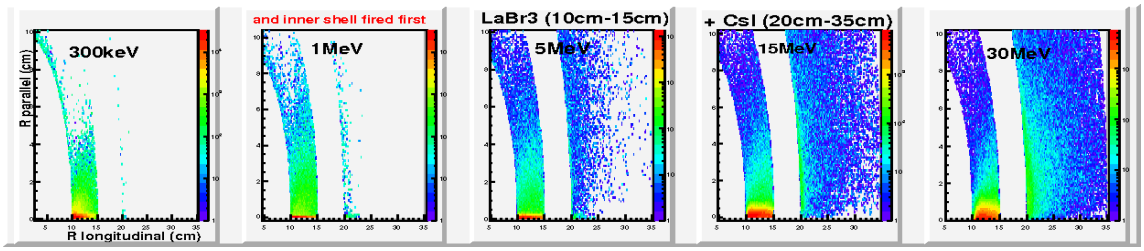

Fig. 16: Identical to Fig.12 for a two-shell geometry with an inner LaBr3 layer with R_{in}=10cm and R_{out}=15cm followed by an outer CsI layer with R_{in}=20cm and R_{out}=35cm.

For the same geometrical configurations than above, Fig.17-21 show the quantity $R_{//}= r \sin\vartheta$ at the relevant frontiers delimiting the layers (given along the *x*-axis). That further illustrates how a given radial expansion of the shower at the end of the inner shell translates at the entrance and exit of the outer shell: Do we have, in the outer shell, a simple continuation of the shower which shape is primarily dictated by the inner shell, or, does the distance *d* and the outer shell sizeably modify the geometrical energy deposit pattern ? In the figures, each interaction point is weighted by the percentage of energy deposited at this point with respect

to the incident energy. No condition on the amount of energy deposited in the detector bulk is applied.

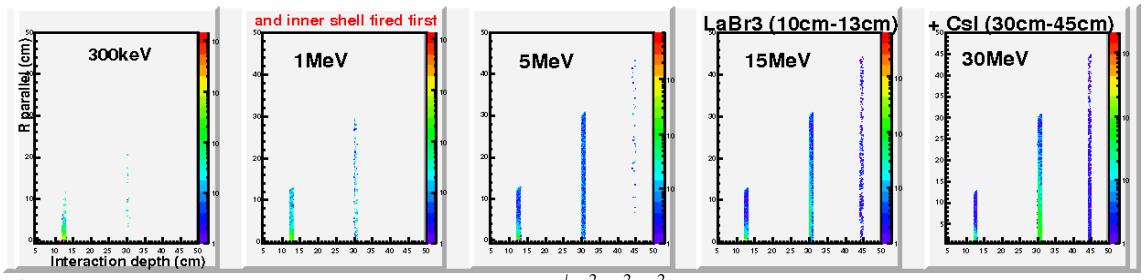

Fig. 17: Correlation between the interaction depth $R=\sqrt{(x^2+y^2+z^2)}$ and the parallel $R_{//}$ radius (both in cm) of all interaction points generated by an incident photon with a given energy. Each point is weighted by the percentage of energy deposit with respect to the incident energy. No condition is required for the amount E_{det} of energy deposited in the detector. The geometry corresponds to a two-shell geometry with an inner LaBr3 layer with R_{in}=10cm and R_{out}=13cm followed by an outer CsI layer with R_{in}=30cm and R_{out}=45cm.

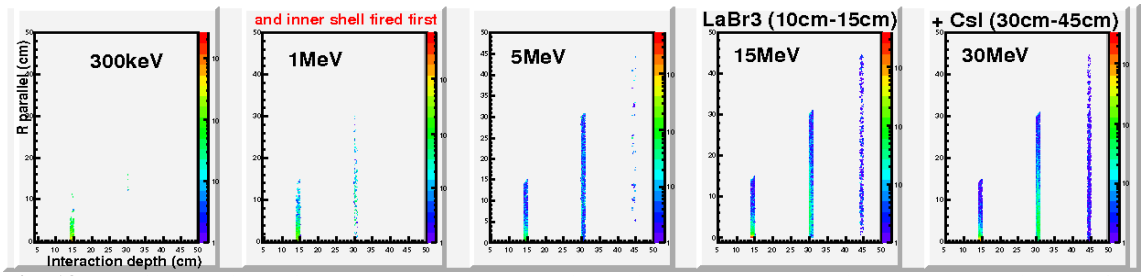

Fig. 18: Identical to Fig.17 for a two-shell geometry with an inner LaBr3 layer with R_{in}=10cm and R_{out}=15cm followed by an outer CsI layer with R_{in}=30cm and R_{out}=45cm.

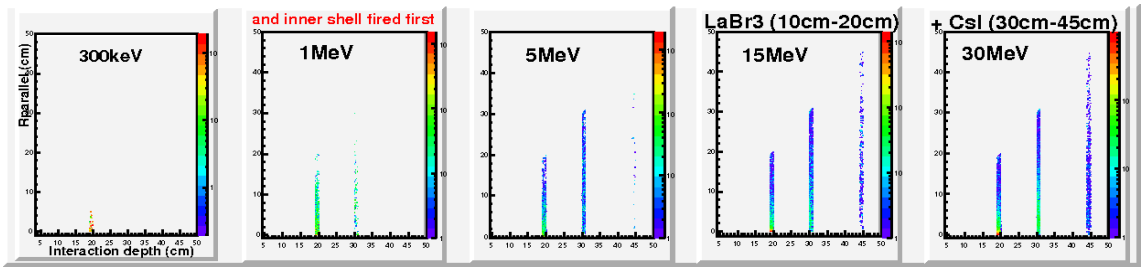

Fig. 19: Identical to Fig.17 for a two-shell geometry with an inner LaBr3 layer with R_{in}=10cm and R_{out}=20cm followed by an outer CsI layer with R_{in}=30cm and R_{out}=45cm.

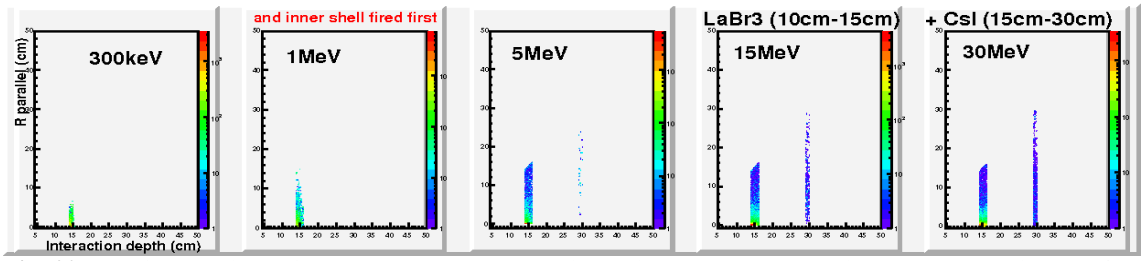

Fig. 20: Identical to Fig.17 for a two-shell geometry with an inner LaBr3 layer with R_{in}=10cm and R_{out}=15cm followed by an outer CsI layer with R_{in}=15cm and R_{out}=30cm.

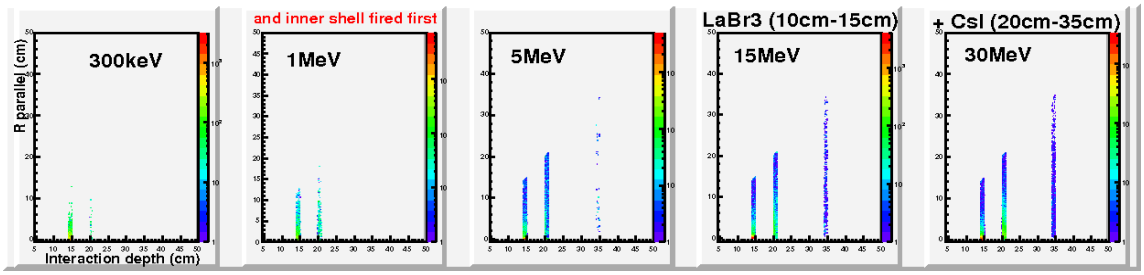

Fig. 21: Identical to Fig.17 for a two-shell geometry with an inner LaBr3 layer with R_{in}=10cm and R_{out}=15cm followed by an outer CsI layer with R_{in}=20cm and R_{out}=35cm.

Qualitatively, there is a nearby homotetical correlation between the shape of the shower in the inner and outer shell and the distance d. That suggests the dominant role of the inner shell on defining the extension of the shower and energy deposit pattern.

---

[1] Report 1 on the PARIS Calorimeter Simulations (http://nz22-13.ifj.edu.pl/~myalski/paris/news.php?lng=en)